

Article

Tribological Properties of Cr_2O_3 , $\text{Cr}_2\text{O}_3\text{-SiO}_2\text{-TiO}_2$ and $\text{Cr}_2\text{O}_3\text{-SiO}_2\text{-TiO}_2\text{-Graphite}$ Coatings Deposited by Atmospheric Plasma Spraying

Lukas Bastakys ^{1,*}, Liutauras Marcinauskas ^{1,2} , Mindaugas Milieška ², Mitjan Kalin ³  and Romualdas Kėželis ²¹ Department of Physics, Kaunas University of Technology, Studentų Str. 50, LT-51368 Kaunas, Lithuania² Plasma Processing Laboratory, Lithuanian Energy Institute, Breslaujos Str. 3, LT-44403 Kaunas, Lithuania³ Laboratory for Tribology and Interface Nanotechnology, Faculty of Mechanical Engineering, University of Ljubljana, Bogiščićeva 8, 1000 Ljubljana, Slovenia

* Correspondence: lukas.bastakys@ktu.lt or lukas.bastakys@ktu.edu; Tel.: +370-6763-3489

Abstract: In this study, Cr_2O_3 , $\text{Cr}_2\text{O}_3\text{-SiO}_2\text{-TiO}_2$ and $\text{Cr}_2\text{O}_3\text{-SiO}_2\text{-TiO}_2\text{-graphite}$ coatings were formed by atmospheric plasma spraying. The influence of $\text{SiO}_2\text{-TiO}_2$ and $\text{SiO}_2\text{-TiO}_2\text{-graphite}$ reinforcements on the surface morphology, elemental composition, structure and tribological properties of chromia coatings was determined. The friction coefficients and specific wear rates were investigated by a ball-on-flat configuration using 1 N and 3 N loads under dry-lubrication conditions. The addition of $\text{SiO}_2\text{-TiO}_2\text{-graphite}$ resulted in the lowest surface roughness and the most homogenous surface of the coatings. The X-ray diffraction (XRD) measurements demonstrated that all as-sprayed coatings consisted of an eskolaite chromium oxide phase. The results showed that the $\text{Cr}_2\text{O}_3\text{-SiO}_2\text{-TiO}_2$ coating demonstrated the lowest friction coefficient values. The $\text{SiO}_2\text{-TiO}_2$ and $\text{SiO}_2\text{-TiO}_2\text{-graphite}$ additives reduced the specific wear rates of Cr_2O_3 coatings by 30% and 45%, respectively. Additionally, the wear resistance was improved almost 45 times in comparison to the steel substrate.

Keywords: plasma spraying; chromia coatings; graphite; tribological properties; friction coefficient

Citation: Bastakys, L.; Marcinauskas, L.; Milieška, M.; Kalin, M.; Kėželis, R. Tribological Properties of Cr_2O_3 , $\text{Cr}_2\text{O}_3\text{-SiO}_2\text{-TiO}_2$ and $\text{Cr}_2\text{O}_3\text{-SiO}_2\text{-TiO}_2\text{-Graphite}$ Coatings Deposited by Atmospheric Plasma Spraying. *Coatings* **2023**, *13*, 408. <https://doi.org/10.3390/coatings13020408>

Academic Editor: Heping Li

Received: 31 December 2022

Revised: 29 January 2023

Accepted: 3 February 2023

Published: 10 February 2023



Copyright: © 2023 by the authors. Licensee MDPI, Basel, Switzerland. This article is an open access article distributed under the terms and conditions of the Creative Commons Attribution (CC BY) license (<https://creativecommons.org/licenses/by/4.0/>).

1. Introduction

Cr_2O_3 coatings are widely used in various fields in order to reduce the wear of metallic parts and metallic surfaces from corrosion [1–6].

Plasma spraying is one of the commonly used techniques to deposit ceramic coatings, such as aluminum oxide, chromium oxide, titanium oxide, zirconium oxide, etc., on metallic surfaces [2,4,7–10]. The mechanical, tribological, thermal or corrosion properties of sprayed Cr_2O_3 coatings are easily controlled by changing the spraying conditions such as spraying distance, arc current, gas type, gas flow ratio, etc. [2,8,11,12]. Kiilakoski et al. [8] indicated that the surface roughness, hardness, porosity and wear resistance of chromia coatings could be controlled by changing the spray distance, flow rate of air or suspension feed rate.

Another way to improve the hardness and toughness, reduce the friction coefficient, or enhance the wear and corrosion resistance of chromia coatings is to use additive materials. It was demonstrated that TiO_2 , Al_2O_3 , YSZ-SiC or CeO_2 is used to improve the properties of Cr_2O_3 coatings [2,13–18]. Li et al. [14] demonstrated that the addition of TiO_2 up to 32 wt.% will improve the tribological properties under dry friction and oil friction conditions. However, it was found that the friction coefficient of $\text{Cr}_2\text{O}_3\text{-TiO}_2$ coatings in most cases was enhanced from 0.60 up to 0.92 under dry sliding. Our previous investigations [15] indicated that the friction coefficient was reduced, and the specific wear rate decreased from $2.69 \times 10^{-6} \text{ mm}^3/(\text{Nm})$ to $1.54 \times 10^{-6} \text{ mm}^3/(\text{Nm})$ after doping of chromium oxide coating with $\text{SiO}_2\text{-TiO}_2$. Mao et al. [16] observed that the wear rate of the chromium oxide coating was $14.6 \times 10^{-7} \text{ mm}^3/(\text{Nm})$ and, depending on the alumina fraction, varied from 8.2 to $12.9 \times 10^{-7} \text{ mm}^3/(\text{Nm})$ for $\text{Cr}_2\text{O}_3\text{-Al}_2\text{O}_3$ coatings. However, the friction coefficient

values under dry-sliding conditions for Cr_2O_3 and $\text{Cr}_2\text{O}_3\text{-Al}_2\text{O}_3$ coatings remained similar. Bolelli et al. [17] demonstrated that the friction coefficients and wear rates were enhanced with the addition of TiO_2 , Al_2O_3 or ZrO_2 into Cr_2O_3 coatings. Singh et al. [19] showed that the friction coefficient of conventional and nanostructured $\text{Cr}_2\text{O}_3\text{-3\%TiO}_2$ coatings varied between 0.55 and 0.80 depending on the applied loads and sliding distances. Ding et al. [20] showed that the properties of $\text{Cr}_2\text{O}_3\text{-20wt.\% TiO}_2$ coatings could be improved with the addition of CeO_2 . It was obtained that the surface roughness and the porosity were reduced, the bonding strength was enhanced and the friction coefficient was reduced from 0.68 to 0.62 with the addition of CeO_2 into $\text{Cr}_2\text{O}_3\text{-TiO}_2$ coatings. Hashemi et al. [21] obtained that $\text{Cr}_2\text{O}_3\text{-YSZ}$ and $\text{Cr}_2\text{O}_3\text{-YSZ-SiC}$ coatings demonstrated higher porosity, lower bonding strength and slightly higher friction coefficient values, but the wear rate of the coatings was reduced up to three times compared to the Cr_2O_3 coating.

The tribological properties of plasma-sprayed ceramic coatings could be improved with the addition of solid lubricant materials such as graphene nanoplatelets [22,23], carbon nanotubes [24], graphene oxide [25] or graphite [26,27]. It was demonstrated that graphene oxide improved the fracture toughness and reduced the microhardness of alumina-graphene oxide-sprayed coatings [25]. The addition of both carbon nanotubes (CNTs) and graphite nanoparticles (GNPs) increased the hardness, elastic modulus and fracture toughness of alumina coatings [23]. Venturi et al. [22] observed that the wear rate was reduced by ~20%, while the friction coefficient decreased from 0.60 to 0.51 with the incorporation of graphene nanoplatelets into Cr_2O_3 coatings. Bagde et al. [27] indicated that the addition of Ni-graphite into the $\text{Cr}_2\text{O}_3\text{-TiO}_2$ coating decreased the friction coefficient values, while the abrasive wear resistance was enhanced from 1.3 up to 2 times depending on the used loads. Goyal et al. [24] showed that the reinforcement of chromia coatings with carbon nanotubes drastically reduced corrosion rates. The performed studies demonstrated that the incorporation of TiO_2 improves the mechanical and tribological properties of the Cr_2O_3 coatings, but the properties of the coatings are greatly influenced by the concentration of TiO_2 , type of used powder and spraying conditions [13–15,17,19]. Another effective way to improve the tribological properties of ceramic coatings is to introduce carbon-based materials (graphite, graphene, graphene oxide, etc.) into the ceramic matrix [22–27]. It should be noted that studies on the incorporation of carbon-based materials into chromia coatings are very scarce in the scientific literature. In addition, the effect of graphite on the tribological behavior of chromium oxide composite coatings formed by atmospheric plasma spraying using air-hydrogen plasma was not studied previously.

The main aim was to investigate the effect of the addition of $\text{SiO}_2\text{-TiO}_2$ and $\text{SiO}_2\text{-TiO}_2\text{-graphite}$ on the surface morphology, phase structure, elemental composition and tribological properties under the dry sliding of chromium oxide composite coatings deposited by atmospheric plasma spraying.

2. Experimental Section

The plasma torch used for the formation of the coatings was developed at the Lithuanian Energy Institute [28]. The P265GH steel was used as a substrate to deposit the chromium (Cr_2O_3) and chromium composite ($\text{Cr}_2\text{O}_3\text{-SiO}_2\text{-TiO}_2$ and $\text{Cr}_2\text{O}_3\text{-SiO}_2\text{-TiO}_2\text{-graphite}$) coatings. The dimensions of the P265GH steel were: length, 40 mm; width, 10 mm; and thickness, 6 mm. The steel was located on a holder that was cooled by water. The deposition of the coatings was performed using atmospheric pressure air plasma spraying, and the parameters of the process were: arc current, 200 A; total gas flow rate, 3.7 g/s; hydrogen gas, which was used to enhance the degree of melting of the powder particles, 0.053 g/s. Such parameters resulted in ~41.0 kW of torch power and an average temperature of the plasma at the torch nozzle chamber (at the point of powder injection) of 3780 ± 50 K. The average plasma temperature at the torch nozzle exit was 3480 ± 30 K. Coatings were formed as the powders were injected into the plasma by a powder carrier gas (air) at a flow rate of 0.48 g/s. The distance between the plasma torch nozzle outlet and the coating surface was 70 mm, and the spraying duration was 40 s. The MOGUL PC 18

powder (MOGUL METALLIZING GmbH, Kottinbrunn, Austria) of Cr_2O_3 (purity, 99.7%; and mesh size, $45 + 22 \mu\text{m}$) was used to deposit the chromium oxide coatings. Meanwhile, the Cr_2O_3 composite coatings were sprayed using $\text{Cr}_2\text{O}_3\text{-SiO}_2\text{-TiO}_2$ (92/5/3, MOGUL PC 17, mesh size: $45 + 22 \mu\text{m}$, MOGUL METALLIZING GmbH, Kottinbrunn, Austria) powders, in which SiO_2 and TiO_2 were mixed in 5% and 3% by weight, respectively [15]. Graphite powders of nonregular shape (MOLYDUVAL Fondra NS, particle size: $<25 \mu\text{m}$) were also used [29]. The graphite was mixed into the $\text{Cr}_2\text{O}_3\text{-SiO}_2\text{-TiO}_2$ at the weight ratio of 10% to produce $\text{Cr}_2\text{O}_3\text{-SiO}_2\text{-TiO}_2\text{-graphite}$ feedstock powders. The powders were mechanically mixed for 24 hours. All feedstock powders were dried at $\sim 350 \text{ K}$ for at least 18 hours before the plasma spraying. For better adhesion between the coating and the substrate, Al as a bonding layer was deposited.

The top-view morphology of the deposited coatings was investigated by scanning electron microscopy (SEM) (Hitachi S-3400N (Hitachi, Tokyo, Japan)), and the elemental composition was measured using energy-dispersive X-ray spectroscopy (EDS) with a Bruker Quad 5040 spectrometer (AXS Microanalysis GmbH, Billerica, MA, USA). The measurement data were collected and measured from at least five different surface locations with a surface area magnification of $\times 100$. Linear surface roughness was measured using a Mitutoyo SurfTest SJ-210 Series tester (version 2.00 with standard ISO 1997 Mitutoyo, Kawasaki, Japan). The roughness values given are the average of at least 15 separate measurements. The length of one track was 4 mm, the speed of the measurement was 0.50 mm/s, the detector measuring force was 0.75 mN and a diamond tip was used. The calculation of average roughness values (R_a , R_q) was performed by a roughness tester according to the ISO4287:1997 standard. Cut-off λ_c was equal to 0.8 mm. The surface roughness of all coatings was measured at the same conditions.

The phase analysis was carried out by the X-ray diffraction technique (XRD) using the D8 Discover apparatus (Bruker D8 Discover, Billerica, MA, USA) with a $\text{CuK}\alpha$ ($\lambda = 0.154059 \text{ nm}$) cathode. The XRD patterns were recorded under standard Bragg–Brentano configuration in the range of 2θ from 10° to 80° . The diffraction patterns of the coatings were analyzed by DIFFRAC.EVA software. The tribological properties were determined using a CETR-UMT-2 tribometer (CETR, Campbell, CA, USA) and ball-on-flat configuration with 1 N and 3 N loads under dry-sliding conditions. The duration of the tribological tests was 120 min, the sliding speed was 0.1 m/s, and the total covered distance was 720 m. A 10 mm diameter Al_2O_3 ball (grade class 10 and 99.5%) was used as a counterpart, and the stroke length was 5 mm. The specific wear rate was calculated from the linear surface profiles that were obtained with Ambios XP-200 Profiler (Ambios Technology Inc., Santa Cruz, CA, USA). Tribological tests of Cr_2O_3 and chromia composite coatings were performed on two samples of each series, and average values (of at least four measurements) were determined.

3. Results and Discussion

The as-sprayed chromia and chromia composite coatings' surface morphology is shown in Figure 1. It was obtained that the deposited coatings consisted of melted particle regions with partially melted particles. It should be noted that the amount of fully melted particle regions in the $\text{Cr}_2\text{O}_3\text{-SiO}_2\text{-TiO}_2$ coating was slightly higher compared to the Cr_2O_3 coating (Figure 1b,d). Mostly, the surface of the $\text{Cr}_2\text{O}_3\text{-SiO}_2\text{-TiO}_2\text{-graphite}$ coating was even and homogenous (Figure 1e,f). All deposited coatings had a grain structure with a low amount of microcracks and pores (Figure 1). The existence of the microcracks is a result of the rapid solidification of partly or fully melted particles on the substrate [19]. The existence of various-shaped micro-sized particles on the surface when the particles hit the substrate could be related to the splashing of partly molten feedstock particles. The porosity of deposited coatings is related to the existence of coarse and fine pores. It was demonstrated that the coarse porosity in the plasma-sprayed coatings is attributed to structural defects. These defects were created by the incomplete filling of the voids between impacting powder particles to the surface [14,19]. SEM images of surface morphology demonstrated that the

addition of TiO_2 and SiO_2 into Cr_2O_3 powders resulted in the formation of a slightly lower amount of larger-sized voids on the surface.

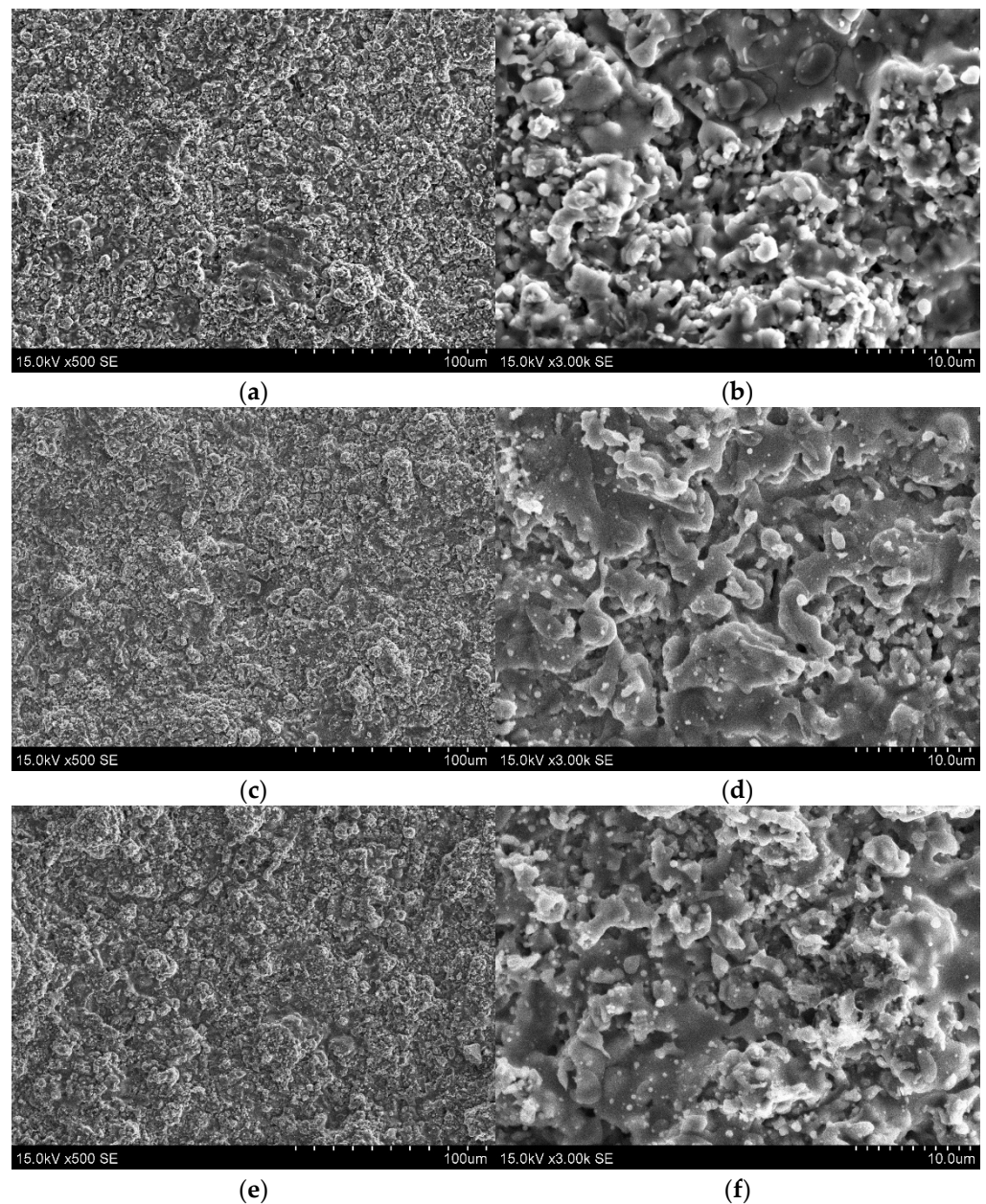


Figure 1. Surface morphology of (a,b) Cr_2O_3 , (c,d) $\text{Cr}_2\text{O}_3\text{-SiO}_2\text{-TiO}_2$ and (e,f) $\text{Cr}_2\text{O}_3\text{-SiO}_2\text{-TiO}_2\text{-graphite}$ coatings.

The distribution of chromium, oxygen, titanium, silicon and carbon on the $\text{Cr}_2\text{O}_3\text{-SiO}_2\text{-TiO}_2$ and $\text{Cr}_2\text{O}_3\text{-SiO}_2\text{-TiO}_2\text{-graphite}$ coatings is presented in Figures 2 and 3. The EDS results showed that the distribution of chromium, oxygen and titanium on the surface of the $\text{Cr}_2\text{O}_3\text{-SiO}_2\text{-TiO}_2$ and $\text{Cr}_2\text{O}_3\text{-SiO}_2\text{-TiO}_2\text{-graphite}$ coatings is homogenous. The EDS map image (Figure 3f) indicated that the graphite particles were quite homogeneously spread on the surface of the as-sprayed coating. In addition, single graphite particles with a size of up to $40\ \mu\text{m}$ could be observed on the surface. It should be noted that silicon tends to agglomerate and form larger clusters on the surface of the chromia composite coatings (Figures 2f and 3e). The existence of larger-sized SiO_2 inclusions is due to the fact that the SiO_2 particles were not homogeneously distributed in the raw powders and/or were agglomerated into bigger-sized clusters during manufacturing. The $\text{Cr}_2\text{O}_3\text{-SiO}_2\text{-TiO}_2$

coating was composed of chromium (~ 73.6 wt.%), oxygen (22.2 wt.%), titanium (3.3 wt.%) and silicon (~ 0.8 wt.%), and a low amount of carbon was obtained due to the absorption of atmospheric air. The as-sprayed coating consisted of Cr (~ 73.7 wt.%), O (~ 21.4 wt.%), Ti (3.0 wt.%), Si (0.8 wt.%) and carbon (~ 1.1 wt.%) when 10 wt.% of graphite was added to the initial Cr_2O_3 - SiO_2 - TiO_2 powders. The EDS measurements showed that the graphite content on the surface was up to 10 times lower compared to the feedstock powders. The chromia coating is composed of chromium (78.3 wt.%) and oxygen (21.3 wt.%), and a low amount of impurities (carbon and aluminum) was detected.

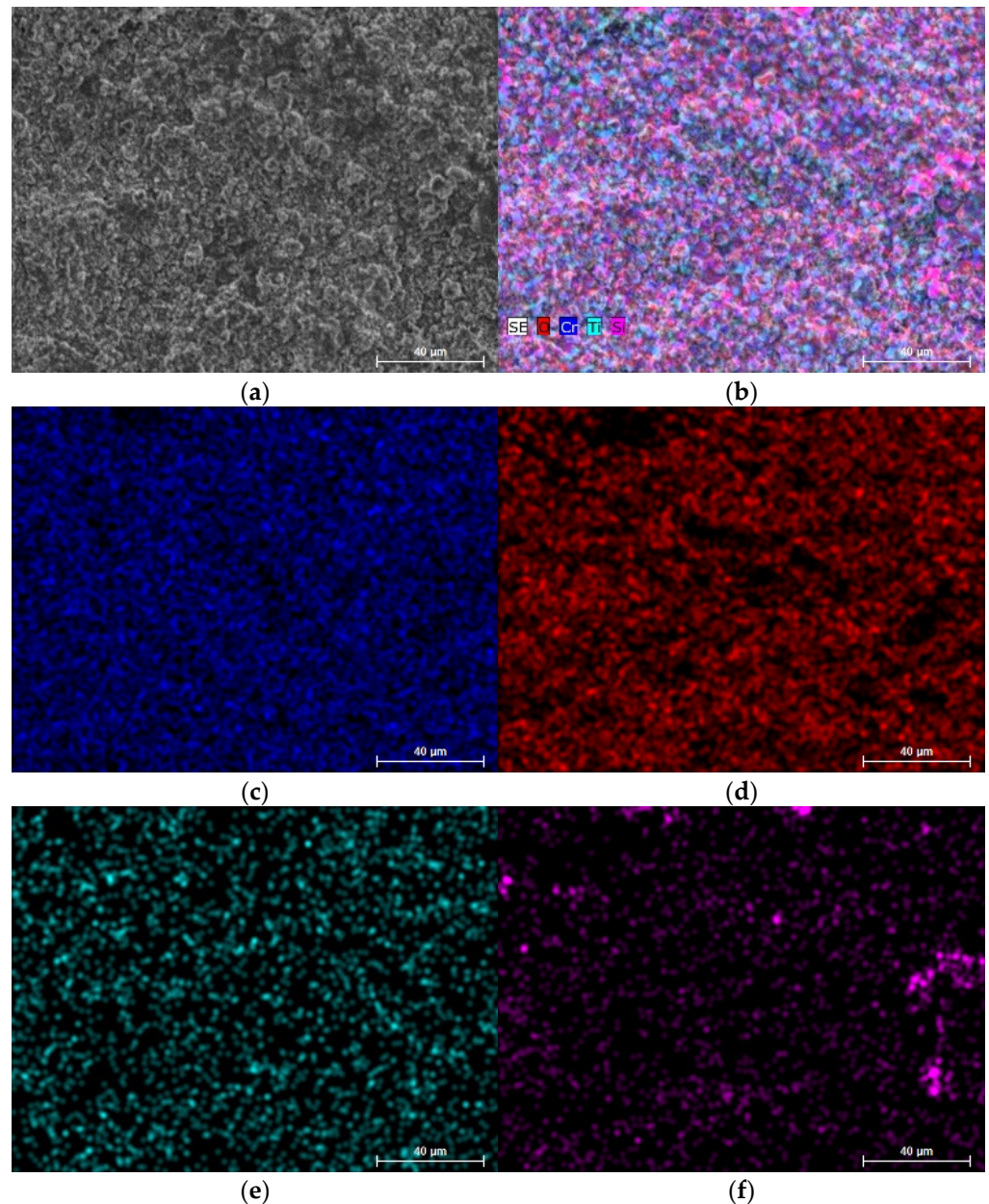


Figure 2. SEM micrograph (a) and elemental maps of Cr_2O_3 - SiO_2 - TiO_2 coating: (b) all elements, (c) chromium, (d) oxygen, (e) titanium and (f) silicon at 500 magnifications.

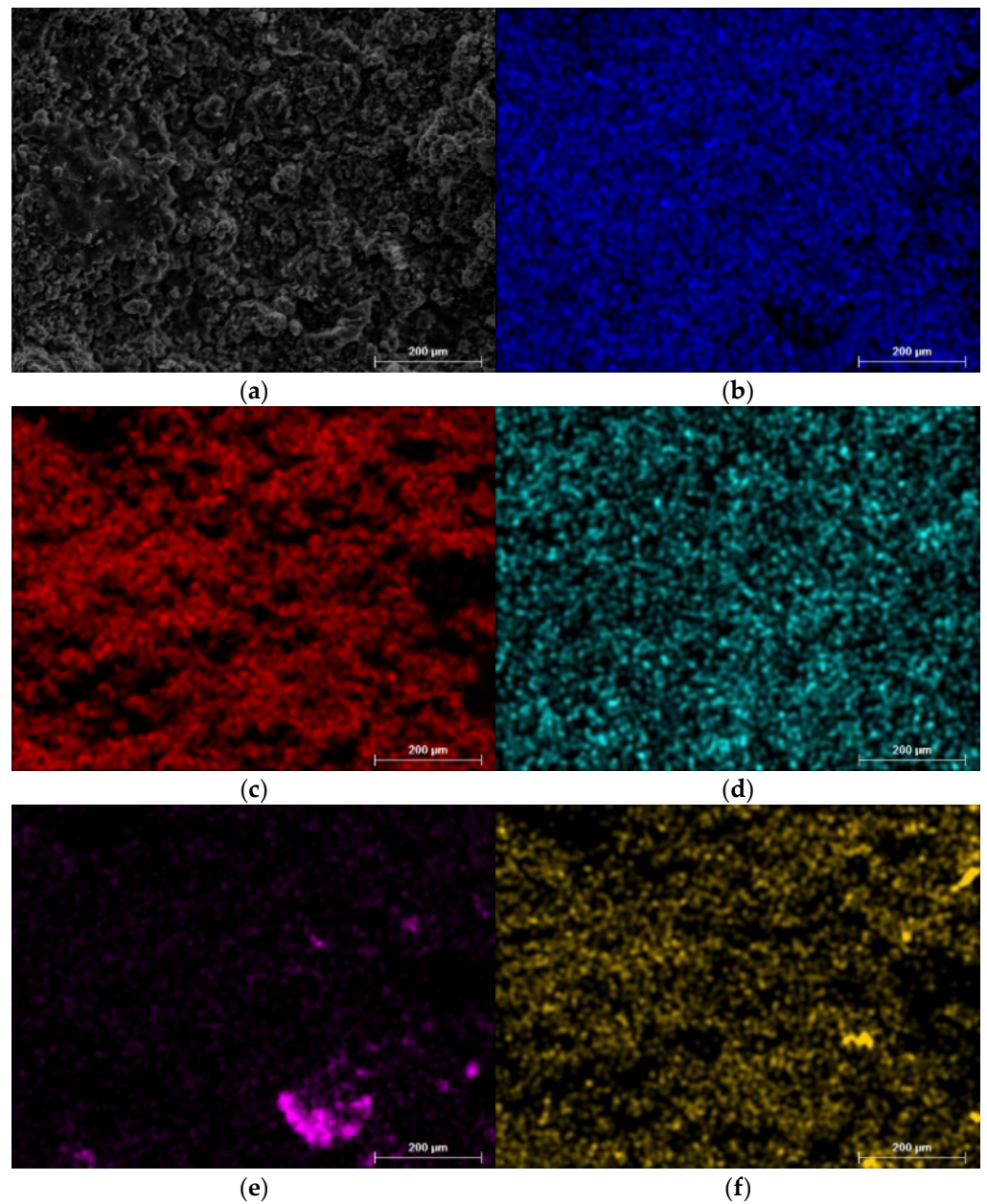


Figure 3. SEM surface image (a) and elemental maps of $\text{Cr}_2\text{O}_3\text{-SiO}_2\text{-TiO}_2\text{-graphite}$ coating: (b) chromium, (c) oxygen, (d) titanium, (e) silicon and (f) carbon at 100 magnifications.

The surface roughness of the as-sprayed coatings is presented in Figure 4. The average surface roughness (R_a) and the root-mean-square roughness (R_q) of the Cr_2O_3 coating were $\sim 3.02 \pm 0.51 \mu\text{m}$ and $\sim 3.77 \pm 0.61 \mu\text{m}$, respectively. The surface roughness of the $\text{Cr}_2\text{O}_3\text{-SiO}_2\text{-TiO}_2$ coating was slightly, up to $\sim 20\%$, higher. The R_a value was $3.85 \mu\text{m}$, while the R_q value was $4.86 \mu\text{m}$. Meanwhile, the roughness of the coating was drastically reduced (by 40%) when 10 wt.% of graphite was added to the $\text{Cr}_2\text{O}_3\text{-SiO}_2\text{-TiO}_2$ powders. The surface roughness R_a and R_q values for the $\text{Cr}_2\text{O}_3\text{-SiO}_2\text{-TiO}_2\text{-graphite}$ coating were $2.22 \mu\text{m}$ and $2.77 \mu\text{m}$, respectively. The reduction of surface roughness of the $\text{Cr}_2\text{O}_3\text{-SiO}_2\text{-TiO}_2\text{-graphite}$ coating in comparison to the $\text{Cr}_2\text{O}_3\text{-SiO}_2\text{-TiO}_2$ coating could be related to the lower size and density of the graphite powders. If we compare the volume of both powders, there were almost equal parts of them in the feedstock mixture.

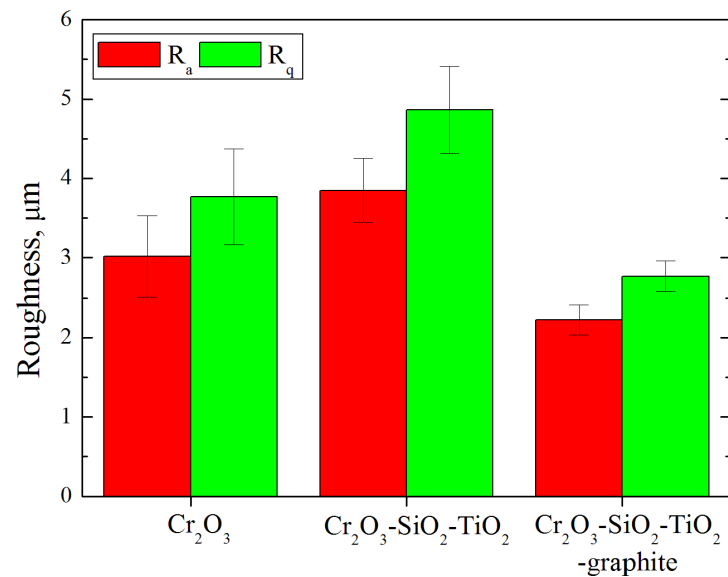


Figure 4. Surface roughness of as-sprayed coatings.

It was demonstrated that the addition of graphite nanoparticles (GNPs) or GNPs and carbon nanotubes (CNTs) into alumina reduced the surface roughness (up to 13%) of the as-sprayed alumina composite coatings [29]. Wang et al. [30] obtained that the addition of 3% or 6% of graphene into Al₂O₃-TiO₂ coatings reduced the porosity of the coatings. In addition, the surface of the coatings becomes flatter and denser after the addition of graphene. Similar results were found for the Cr₂O₃-SiO₂-TiO₂ coating with the addition of graphite into feedstock powders. The surface images of the Cr₂O₃-SiO₂-TiO₂ coating demonstrated that the amount of fully molten regions was higher compared to the Cr₂O₃ coating. However, the surface roughness of the Cr₂O₃-SiO₂-TiO₂ coating was enhanced. Zamani et al. [2] also obtained that the surface roughness of the Cr₂O₃ coating was lower compared to Cr₂O₃-SiO₂-TiO₂ coatings. However, the surface roughness was reduced with the increased amount of Al₂O₃ due to the lower melting temperature. The fraction of splats increases on the surface of deposited chromia or chromia composite coatings with the increase of the plasma jet temperature or supplementation of the metal oxides with lower melting temperature into feedstock powders [11,15,16,31].

The XRD graphs of the Cr₂O₃ and Cr₂O₃ composite coatings are given in Figure 5. It should be noted that the patterns of all coatings showed the same peaks, and only the intensities of the peaks are slightly different. The peaks are located at 24.6, 33.7, 36.3, 41.6, 50.3, 55.0, 63.6, 65.3 and 73.1 2θ degrees and are attributed to the (012), (104), (110), (202), (024), (116), (214), (300) and (1010) orientations of the Cr₂O₃ eskolaite phase, respectively [10,14,15,32]. The low- and broad-intensity peaks located at ~40.0°, ~44.4°, ~58.5°, and ~76.9° are assigned to the (006), (202), (122) and (220) planes of the eskolaite Cr₂O₃ phase, respectively [14,15,23]. The normalized intensities of the initial powders and as-sprayed coatings are presented in Table 1. It should be noted that the highest-intensity peak for the initial Cr₂O₃ powders was located at ~55.0°. Meanwhile, the as-sprayed chromia coatings had the highest peak at ~33.7°. The intensity of the peak at ~36.3° was slightly lower. It should be noted that the intensities of dominant peaks of the eskolaite Cr₂O₃ phase increased in the as-sprayed Cr₂O₃ coating (Table 1). The highest-intensity peak for the Cr₂O₃ coating was related to the (104) orientation (Figure 5). The addition of SiO₂-TiO₂ into the Cr₂O₃ coatings resulted in the intensity of the peak presented at ~33.7° (104) being slightly lower compared to the peak located at ~36.3° (110). The intensities of peaks for the Cr₂O₃-SiO₂-TiO₂-graphite and Cr₂O₃-SiO₂-TiO₂ coatings were similar (Figure 5). The highest-intensity peak in the Cr₂O₃-SiO₂-TiO₂ feedstock powders was obtained at ~36.3°. The order of the five highest peaks according to normalized intensity remains unchanged in the as-sprayed Cr₂O₃-SiO₂-TiO₂ coating. Only a slight increase or decrease in

the peak intensities was obtained (Table 1.). The addition of graphite into $\text{Cr}_2\text{O}_3\text{-SiO}_2\text{-TiO}_2$ resulted only in a slight reduction in the intensities of most peaks. However, the intensities of the peaks at $\sim 41.6^\circ$ and $\sim 63.6^\circ$ were enhanced for the $\text{Cr}_2\text{O}_3\text{-SiO}_2\text{-TiO}_2\text{-graphite}$ coating.

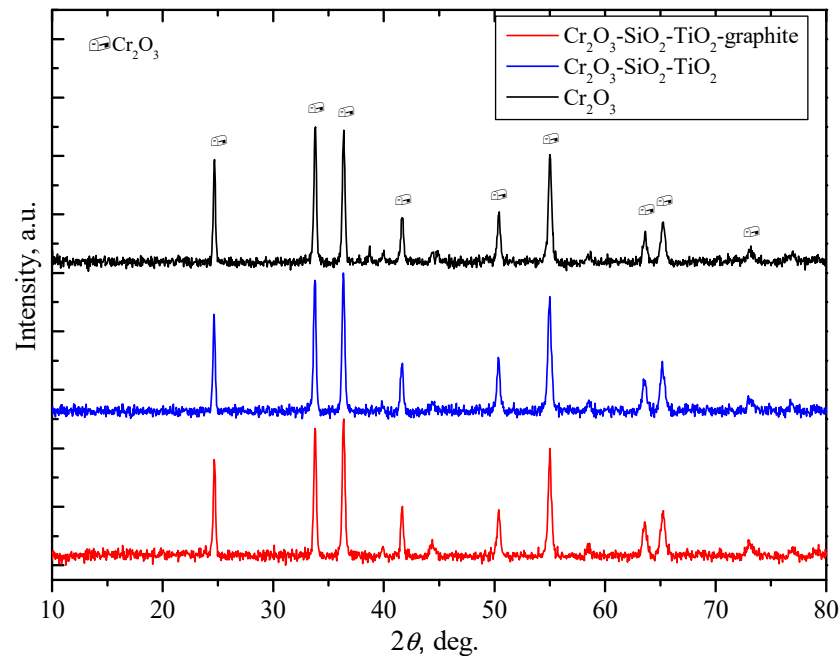


Figure 5. The XRD patterns of the Cr_2O_3 , Cr_2O_3 , $\text{Cr}_2\text{O}_3\text{-SiO}_2\text{-TiO}_2$ and $\text{Cr}_2\text{O}_3\text{-SiO}_2\text{-TiO}_2\text{-graphite}$ coatings.

Table 1. The normalized intensity values of XRD peaks in the powders and coatings.

Peak Position, $^\circ$	Normalized Intensities Values				
	Cr_2O_3 Powders	$\text{Cr}_2\text{O}_3\text{-SiO}_2\text{-TiO}_2$ Powders	Cr_2O_3 Coating	$\text{Cr}_2\text{O}_3\text{-SiO}_2\text{-TiO}_2$ Coating	$\text{Cr}_2\text{O}_3\text{-SiO}_2\text{-TiO}_2\text{-Graphite}$ Coating
24.6	0.446 ⁴	0.784 ⁴	0.763 ⁴	0.721 ⁴	0.710 ⁴
33.7	0.756 ²	0.933 ²	1.000 ¹	0.947 ²	0.933 ²
36.3	0.500 ³	1.000 ¹	0.955 ²	1.000 ¹	1.000 ¹
40.0	0.247	0.165	0.090	0.085	0.080
41.6	0.162	0.343	0.340	0.332	0.364 ⁵
50.3	0.392 ⁵	0.520 ⁵	0.360 ⁵	0.370 ⁵	0.337
55.0	1.000 ¹	0.836 ³	0.795 ³	0.815 ³	0.780 ³
63.6	0.257	0.161	0.223	0.228	0.261
65.3	0.311	0.206	0.305	0.352	0.340

Superscripts indicate order of normalized peak intensities, lower numbers attributed to higher intensity.

The TiO_2 or SiO_2 phases were not detected in the XRD data of the $\text{Cr}_2\text{O}_3\text{-SiO}_2\text{-TiO}_2$ and $\text{Cr}_2\text{O}_3\text{-SiO}_2\text{-TiO}_2\text{-graphite}$ coatings. Usually, the presence of the TiO_2 rutile phase in the XRD patterns of thermally sprayed coatings is attributed to peaks located at 27.5 , 41.3 , 54.4 and 56.7° [10,14,19]. However, it was observed that the TiO_2 rutile phase may not be detected in the XRD data of the chromia composite coatings with a low amount of TiO_2 (up to 5%) [32]. The crystalline graphite peak (at 26.5°) was not obtained in the XRD pattern of the $\text{Cr}_2\text{O}_3\text{-SiO}_2\text{-TiO}_2\text{-graphite}$ coating [26,33]. Our previous study [26] demonstrated that the low-intensity crystalline graphite peak in alumina-graphite coatings was observed when the graphite content was 1.6 wt.%.

The variation of the friction coefficient curves depending on sliding time is given in Figure 6. Similar behavior of the friction coefficient curves was obtained for all as-sprayed coatings. The average values of the friction coefficient for the Cr_2O_3 , $\text{Cr}_2\text{O}_3\text{-SiO}_2\text{-TiO}_2$ and $\text{Cr}_2\text{O}_3\text{-SiO}_2\text{-TiO}_2\text{-graphite}$ coatings using 1 N load were estimated as ~ 0.369 , ~ 0.316 and

~ 0.405 , respectively (Figure 7a). The friction coefficient of the steel substrate was ~ 0.687 when 1 N load was used [15]. The friction coefficients of the coatings slightly increased with the enhancement of the applied load (Figure 7a). The lowest friction coefficient was obtained for the $\text{Cr}_2\text{O}_3\text{-SiO}_2\text{-TiO}_2$ coating and was ~ 0.378 . Meanwhile, the highest value of the friction coefficient (~ 0.416) was observed for the $\text{Cr}_2\text{O}_3\text{-SiO}_2\text{-TiO}_2\text{-graphite}$ coating. Thus, the friction coefficient slightly decreased (by 2%) when the $\text{SiO}_2\text{-TiO}_2$ additive was used. Meanwhile, the addition of $\text{SiO}_2\text{-TiO}_2\text{-graphite}$ fractionally increased (up to 8%) the friction coefficient of the Cr_2O_3 composite coatings. Despite the fact that the friction coefficient of all the coatings increased with the increase in the applied load, it was significantly lower (up to 40%) than that of the P265GH steel (~ 0.630).

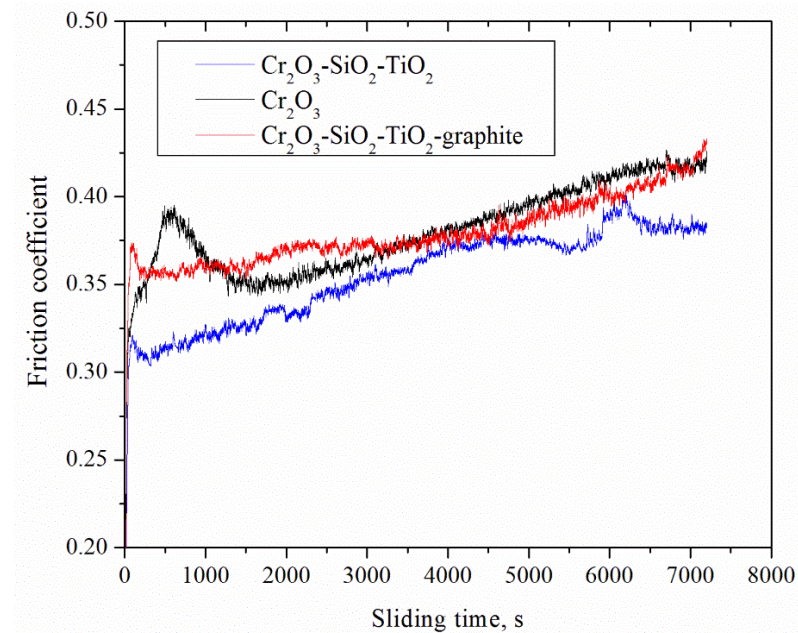


Figure 6. The variation of friction coefficients of coatings versus sliding time when 3 N load was used.

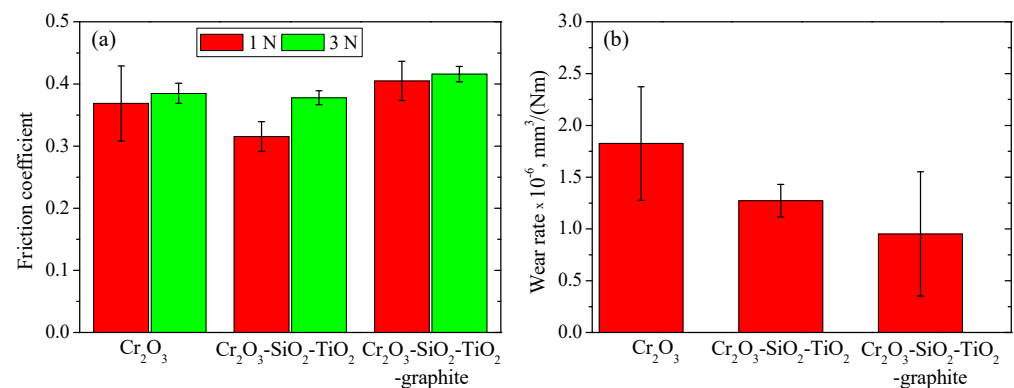


Figure 7. Friction coefficients of deposited coatings (a) and the specific wear rates of coatings when 3 N load was applied (b).

It was demonstrated that the addition of a low amount of graphene oxide could reduce the friction coefficient of alumina coatings by 15%. However, the friction coefficient could also be enhanced from 0.49 to 0.52 with the increase in the used load [34]. Priyadershini et al. [29] observed that the addition of a low amount of GNPs and CNTs into alumina coatings resulted in a higher friction coefficient at the initial (up to 300 m) sliding distances. It was obtained that the friction coefficient depends on the applied load, type of used counterpart, porosity, hardness, surface roughness of the material, etc. [11,14,21,34,35]. Liang et al. [35] observed that the average friction coefficient decreased with the increase in

the initial roughness values of the material. Riedl et al. [36] determined that the friction coefficient of Al_2O_3 coating with the alpha phase was slightly reduced after surface polishing. Meanwhile, the friction coefficient of the Al_2O_3 coating with the kappa phase demonstrated an opposite trend. The steady state of the friction coefficient for the Cr_2O_3 coating was reached after 1500 s of sliding time, while the steady state for the Cr_2O_3 - SiO_2 - TiO_2 -graphite coating was reached after 200–300 s. The surface with a larger initial roughness will need more time to reach the steady friction coefficient values, because the sharp hilltops must be grounded off first [35,36]. In addition, the smoother the surface, the greater the contact area between the friction pair, which can lead to higher friction coefficient values. The slight increase in the friction coefficient versus time for ceramic coatings and ceramic-carbon-based coatings during the steady-state region was observed in several studies when dry-sliding and different loads were used [11,14,30,34].

The average specific wear rates of the deposited coatings using 3 N load are presented in Figure 7b. The wear rate of the chromium oxide coating was $\sim 1.83 \times 10^{-6} \text{ mm}^3/(\text{Nm})$. The specific wear rate decreased to $\sim 1.27 \times 10^{-6} \text{ mm}^3/(\text{Nm})$ with the addition of SiO_2 - TiO_2 into the chromium oxide powders. The addition of the graphite in the feedstock powders stipulated the formation of the coating with the lowest specific wear rate of $\sim 0.95 \times 10^{-6} \text{ mm}^3/(\text{Nm})$. It should be mentioned that the specific wear rates of the P265GH steel were $6.68 \times 10^{-5} \text{ mm}^3/(\text{Nm})$ and $4.22 \times 10^{-5} \text{ mm}^3/(\text{Nm})$ when 1 N and 3 N loads were used, respectively. The reduction of the wear rate of the chromia composite coatings could be attributed to the enhanced densification, reduction of porosity, presence of transferred layer from the Al_2O_3 ball and formation of self-lubricating graphite layer (in the case of Cr_2O_3 - SiO_2 - TiO_2 -graphite) [29,33]. The increase in the sliding wear rates of the Cr_2O_3 coatings with the incorporation of TiO_2 compared to the Cr_2O_3 coatings during the sliding tests against an Al_2O_3 counterpart was noticed by several authors [13,17,19,37,38]. It was obtained that the reinforcement of TiO_2 decreased the hardness, and as a result, the resistance to wear of the Cr_2O_3 - TiO_2 coatings was reduced [13].

The wear tracks of the chromium oxide and its composite coatings under the loads of 1 N and 3 N are presented in Figure 8. It should be noted that the surface of the as-sprayed coatings was only slightly damaged when 1 N load was applied (Figure 8a,c,e). The randomly distributed worn areas of 10 μm to 30 μm in size could be seen on the surfaces. The surface profile measurements demonstrated similar profiles as for deposited coatings. Thus, it was not possible to calculate the wear rates of the as-sprayed coatings, as only the top hills were fractionally abraded when tribological tests were performed using a load of 1 N. Meanwhile, the specific wear rate of the steel substrate under 1 N load was $6.68 \times 10^{-5} \text{ mm}^3/(\text{Nm})$. Compared with 1 N, and with the increased load up to 3 N, the interfacial contact area of the coatings increased. The SEM images indicated that the wear scars became wider, brighter and more worn-out areas were observed (Figure 8). These results indicate that the damage level and wear loss increased and resulted in a higher wear rate of the coatings.

The distribution of chemical elements on the wear scars of the coatings after tribological tests using 3 N load is presented in Figures 9–11. A low amount of aluminum from the alumina ball was obtained on the worn scars of all coatings (Figures 9e, 10e and 11e). Additionally, due to the heat generated during the sliding process, the small concentrations of carbon at a contact zone were determined (Figures 9f and 10f). The EDS results showed that the concentration of chromium was $\sim 71.6 \text{ wt.}\%$, oxygen $\sim 27.1 \text{ wt.}\%$, aluminum 0.9 wt.% and carbon 0.4 wt.% on the wear tracks of the chromia coating after the tribological tests with 3 N load. The amount of Cr was $\sim 67.7 \text{ wt.}\%$, O—26.4 wt.%, Ti—3.0 wt.%, Si—1.5 wt.%, C—0.5 wt.% and Al—0.9 wt.% on surface of the Cr_2O_3 - SiO_2 - TiO_2 coating. The concentration of chromium was $\sim 68.7 \text{ wt.}\%$, oxygen $\sim 25.4 \text{ wt.}\%$, titanium $\sim 2.7 \text{ wt.}\%$, silicon $\sim 0.7 \text{ wt.}\%$, aluminum 1.1 wt.% and carbon 1.4 wt.% on the wear track of the Cr_2O_3 - SiO_2 - TiO_2 -graphite coating. The increase in the oxygen concentration and the reduction of chromium amount on the wear scars for all coatings were observed after the tribological

tests. The slight oxidation of chromia ceramic coatings after tribological tests was observed by Amanov et al. [18] and is a result of abrasive wear.

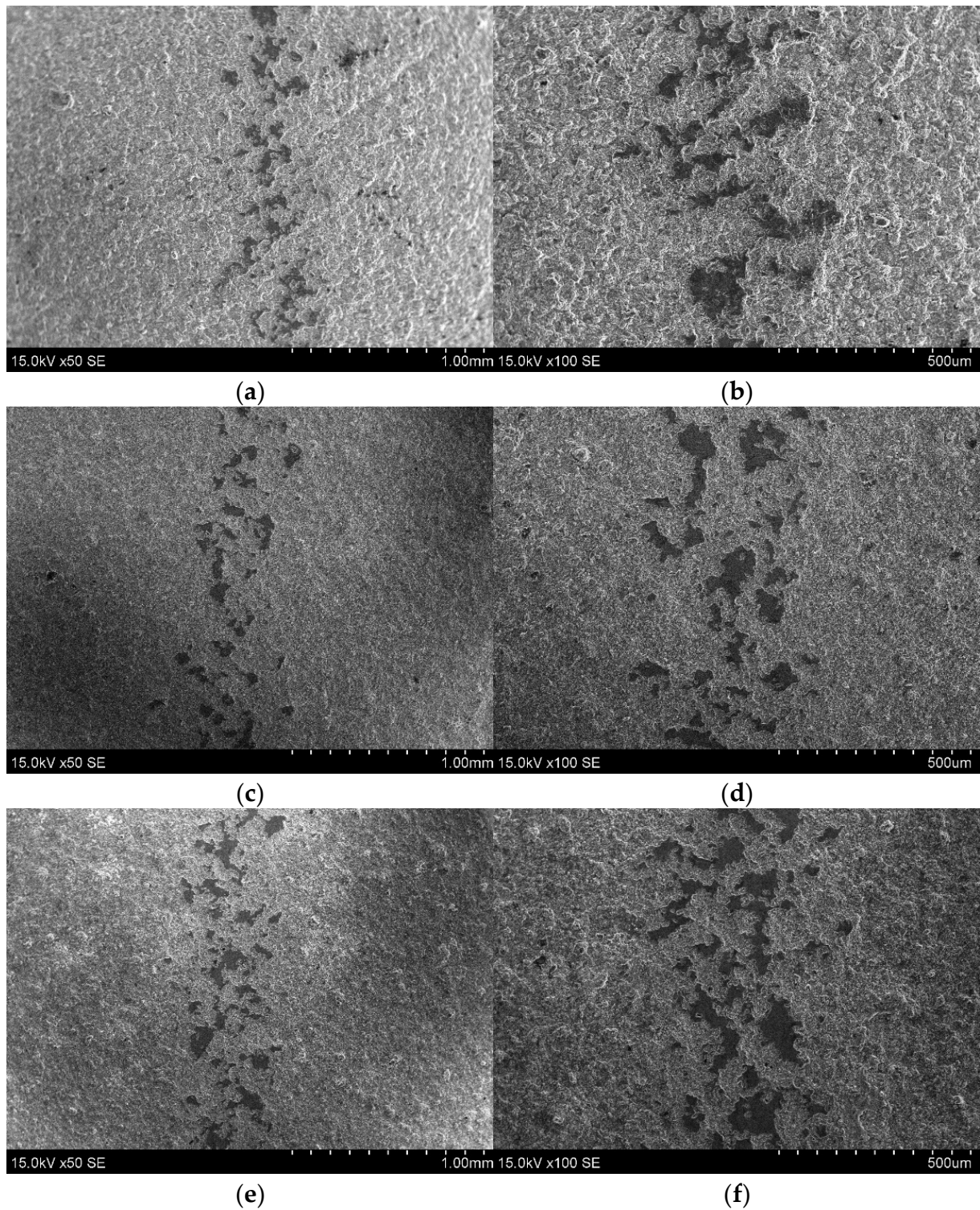


Figure 8. Wear scars views of (a,b) Cr₂O₃, (c,d) Cr₂O₃-SiO₂-TiO₂ and (e,f) Cr₂O₃-SiO₂-TiO₂-graphite coatings after tribological tests with (a,c,e) 1 N and (b,d,f) 3 N loads.

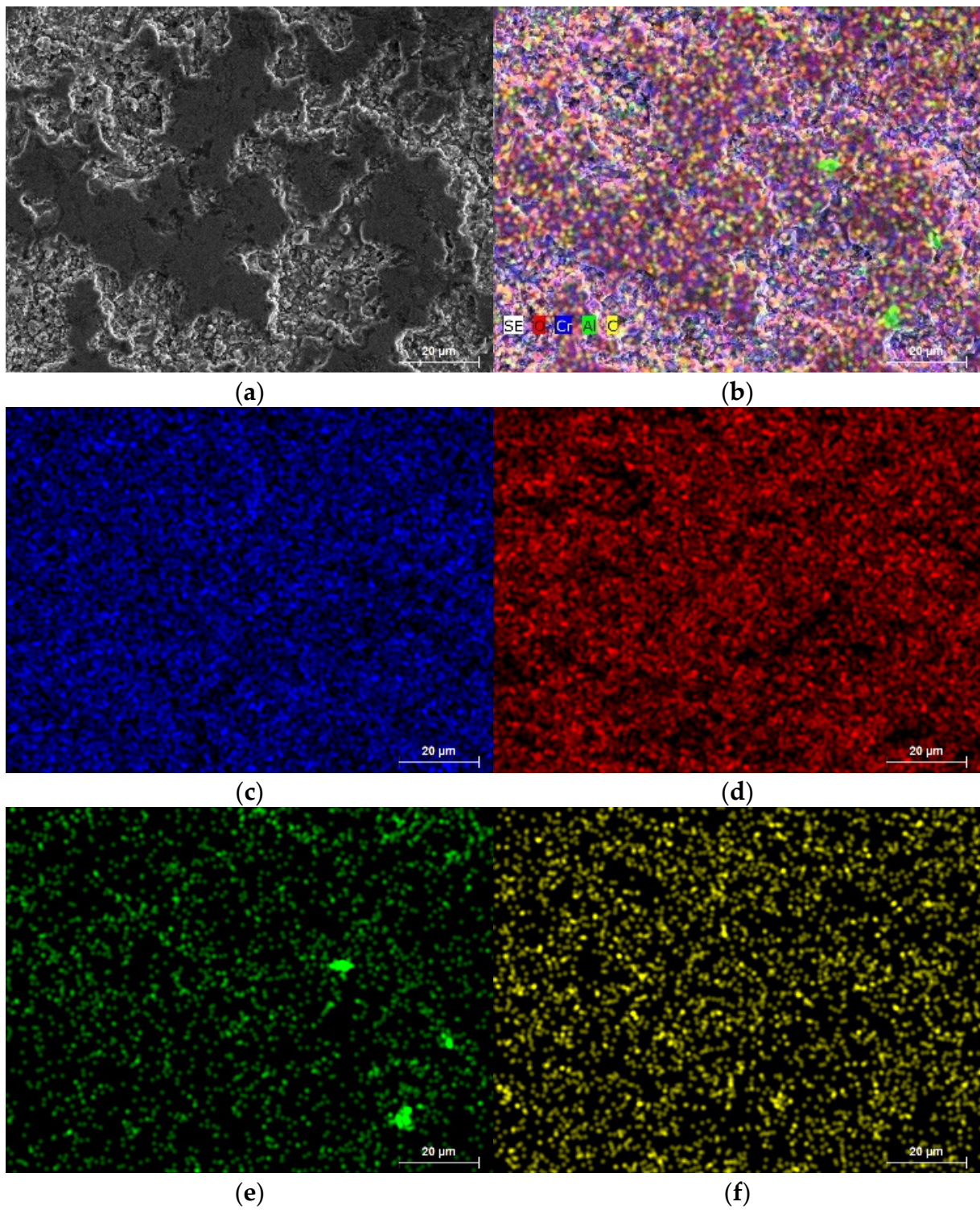


Figure 9. SEM (a) and EDS mapping images of worn surface of Cr_2O_3 coating, all detected elements (b), chromium (c), oxygen (d), aluminum (e) and carbon (f) on the wear scar surface of Cr_2O_3 coating.

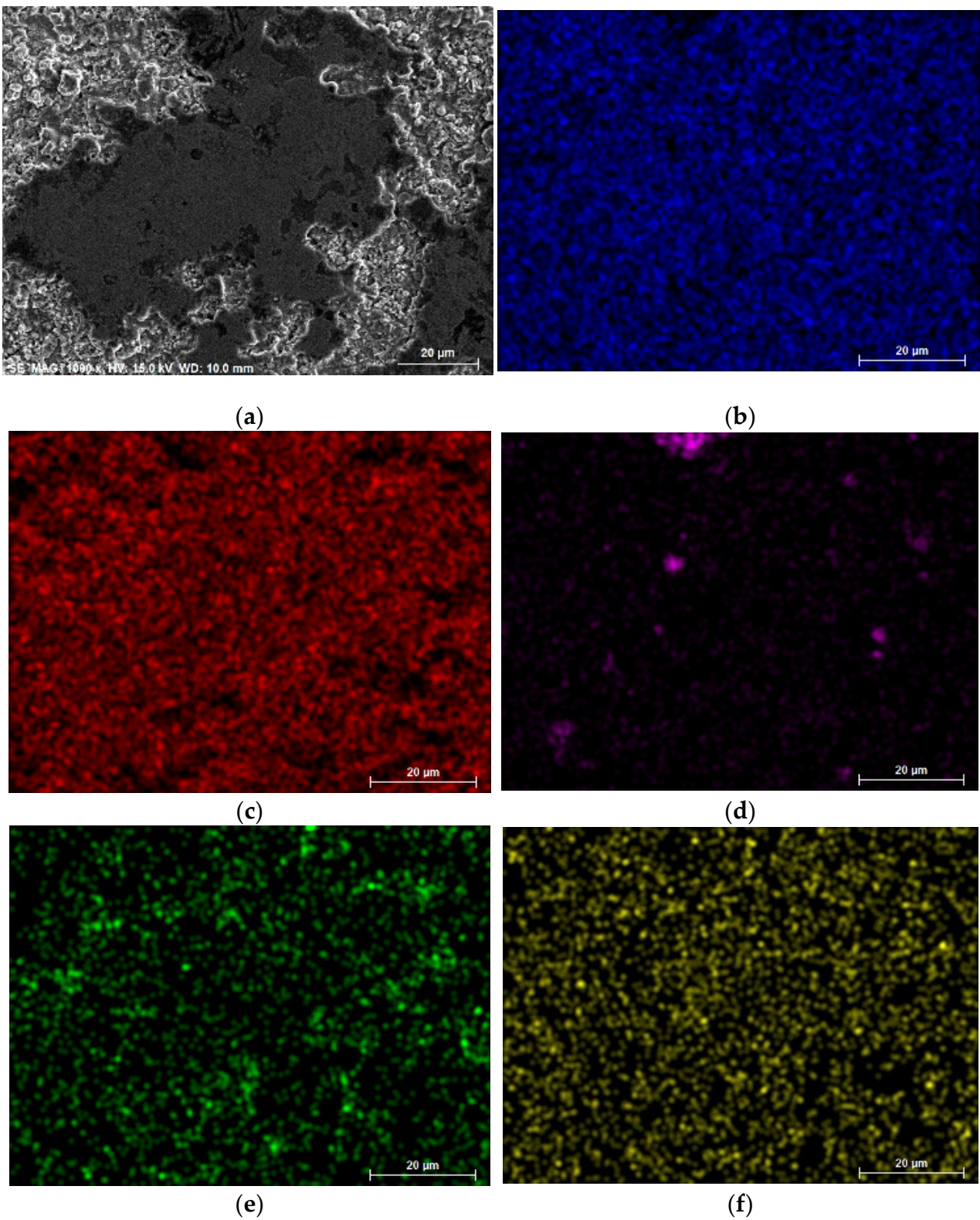


Figure 10. SEM (a) and EDS mapping images of worn surface of $\text{Cr}_2\text{O}_3\text{-SiO}_2\text{-TiO}_2$ coating, Cr (b), O (c), Si (d), Al (e) and C (f).

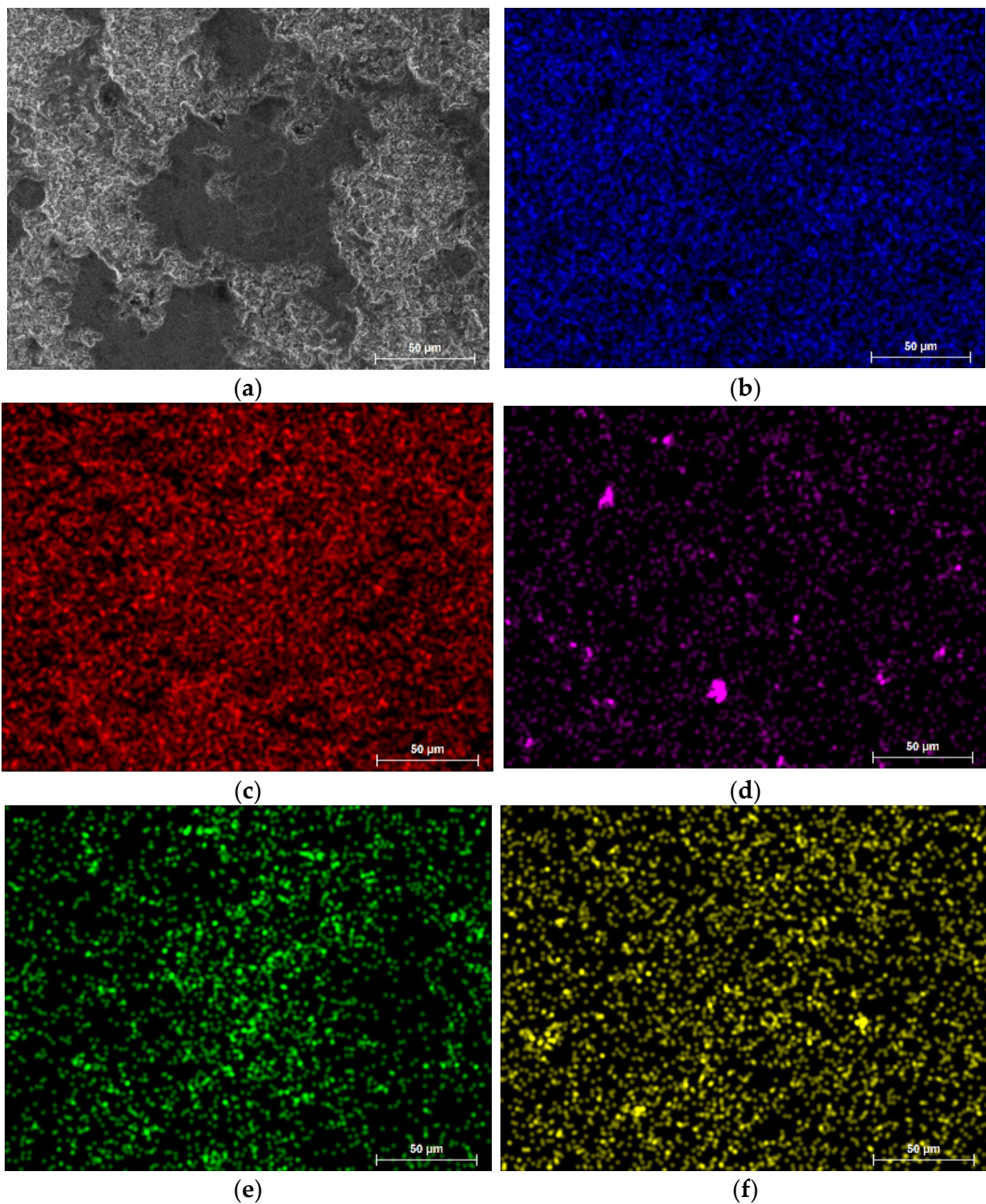


Figure 11. SEM (a) and EDS mapping images of worn surface of $\text{Cr}_2\text{O}_3\text{-SiO}_2\text{-TiO}_2\text{-graphite}$ coating, Cr (b), O (c), Si (d), Al (e) and C (f) when 3 N load was used.

The EDS results indicated the presence of Al and an increase in carbon elemental concentration in the worn surfaces of the coatings after the tribological tests. A low amount of aluminum was (from 0.9 wt.% to 1.1 wt.%) observed for all coatings after the tribological tests. This confirms the formation of the tribolayer of Al and is a result of the wear between the counterpart (Al_2O_3 ball) and coating [34]. The existence of carbon

indicates the formation of a graphite-base film on the surface of the removed areas [26,33]. The graphite may act as a solid lubricant to prevent the direct contact between the Al_2O_3 ball and the surface of the coating. The SEM images indicated that the wear scars are noncontinuous (Figure 8). Thus, effective lubrication would be provided only in the direct contact zone. The EDS results and mapping images indicated that the amount of carbon at the wear scar areas increased from ~ 1.1 to ~ 1.4 wt.%. Feng et al. [33] demonstrated that the GNPs and graphite particles start to act as a self-lubricant, and a stable tribofilm layer is formed on the surface of the Al_2O_3 - TiO_2 coatings when the applied loads are 15 N or higher. Thus, the friction coefficient values would remain similar or even higher compared to the Cr_2O_3 - SiO_2 - TiO_2 coating. In our case, the used 1 N and 3 N loads in tribological tests are considered as light loads. Thus, the wear volume was very low (see Figure 8), and the graphite particles could not be effectively pulled out from the Cr_2O_3 - SiO_2 - TiO_2 -graphite coating to act as a self-lubricant.

Wear debris in the form of small microsized particles was obtained on the surfaces of the coatings. The size of the debris was very similar for all coatings. Usually, the interfacial bonding between the formed splat starts to delaminate at higher loads or longer sliding distances. However, the lamellar debris was not produced under used loads. Severe abrasive wear is probably the main wear mechanism during the dry-sliding tests. As for the single one, parallel grooves can be obtained on the wear tracks of the coatings [18,27,39,40]. The particles are extracted from the coating and are crushed in the contact zone between the surface of the coating and the sliding Al_2O_3 ball. The pulled-out TiO_2 or TiO_2 -graphite particles start to form a lubricative layer and improve the tribological properties (especially wear rate). Meanwhile, the hard Cr_2O_3 particles act as an abrasive and can tear up the formation of the tribolayer. The traces of Al on the worn surfaces also indicate that the Al_2O_3 ball slightly rubs and wears and could be involved in the formation of the tribolayer. The increase in the graphite amount on the wear scars is evidence of the initial tribofilm formation. It was reported that the graphite layer led to the reduction of the shear stress level and plastic deformation in the contact zone, which reduces the wear rate of ceramic coatings [27,39].

The tribological investigations demonstrated that the addition of SiO_2 - TiO_2 and SiO_2 - TiO_2 -graphite additives had an insignificant effect on the friction coefficient of the chromia coating when 3 N load was used. However, the wear resistance of the chromia composite coatings under dry-sliding conditions was improved by up to $\sim 45\%$ compared to the chromia coating.

4. Conclusions

Cr_2O_3 and chromia composite coatings were formed by atmospheric plasma spraying. The addition of SiO_2 - TiO_2 enhanced (up to 20%) while the SiO_2 - TiO_2 -graphite additive decreased (25%) the surface roughness compared to the Cr_2O_3 coating. The addition of graphite increased the homogeneity of the surface and enhanced the amount of molten areas on the surface of the Cr_2O_3 - SiO_2 - TiO_2 -graphite coating. The concentration of carbon in the as-sprayed coating was only ~ 1.1 wt.%, indicating that most of the graphite was lost in the plasma flow due to sublimation. The XRD results indicated that the Cr_2O_3 , Cr_2O_3 - SiO_2 - TiO_2 and Cr_2O_3 - SiO_2 - TiO_2 -graphite coatings consisted only of the eskolaite phase. The lowest friction coefficient values of 0.316 and 0.378 were observed for the Cr_2O_3 - SiO_2 - TiO_2 coating when the friction tests were carried out using 1 N and 3 N, respectively. The amount of carbon on the wear scars was ~ 1.4 wt.%, which is $\sim 25\%$ higher compared to the as-sprayed coating. This indicates the formation of the self-lubricating layer on the surface. However, the applied loads were too low for the formation of the continuous wear tracks, and the effect of graphite as a solid lubricant was limited. The friction coefficient of the coatings was lower by 40% in comparison to the steel under dry-sliding conditions. The wear resistance of the Cr_2O_3 coatings was enhanced by $\sim 30\%$ and $\sim 45\%$ with the addition of SiO_2 - TiO_2 and SiO_2 - TiO_2 -graphite, respectively. The improvement in tribological properties of the Cr_2O_3 composite coatings could be related to a higher amount of molten particle

areas on the surface due to the lower melting temperatures of SiO₂ and TiO₂. The lowest specific wear rate of $0.95 \times 10^{-6} \text{ mm}^3/(\text{Nm})$ was reached for the Cr₂O₃-SiO₂-TiO₂-graphite coating, which was considerably lower (up to 45 times) compared to the steel value.

Author Contributions: Conceptualization, L.B. and L.M.; methodology, L.B., M.M., R.K. and M.K.; software, L.B.; validation, L.B. and M.M.; formal analysis, L.B. and L.M.; investigation, L.B., L.M., M.M., R.K. and M.K.; data curation, L.B.; writing—original draft preparation, L.B., M.M. and L.M.; writing—review and editing, L.B. and L.M.; visualization, L.B. and L.M.; supervision, L.B.; All authors have read and agreed to the published version of the manuscript.

Funding: This research received no external funding.

Institutional Review Board Statement: Not applicable.

Informed Consent Statement: Not applicable.

Data Availability Statement: Not applicable.

Acknowledgments: The authors thank M. Grigaliūnas from the Kaunas University of Technology and S. Matkovič from the University of Ljubljana for tribological measurements.

Conflicts of Interest: The authors declare no conflict of interest.

References

1. Ratia, V.; Zhang, D.; Daure, J.; Shipway, P.; McCartney, D.; Stewart, D. Sliding wear of a self-mated thermally sprayed chromium oxide coating in a simulated PWR water environment. *Wear* **2019**, *426*, 1466–1473. [\[CrossRef\]](#)
2. Zamani, P.; Valefi, Z.; Jafarzadeh, K. Comprehensive study on corrosion protection properties of Al₂O₃, Cr₂O₃ and Al₂O₃-Cr₂O₃ ceramic coatings deposited by plasma spraying on carbon steel. *Ceram. Int.* **2021**, *48*, 1574–1588. [\[CrossRef\]](#)
3. Lee, D.; Tucker, J.R.C.; Crawmer, D.E.; Karthikeyan, J.; Sanpo, N.; Wang, J.; Berndt, C.C.; Knapp, J.; Lemen, D.; Riggs, W.; et al. Wear-Resistant Coatings. *ASM Int.* **2013**, *5*, 253–256. [\[CrossRef\]](#)
4. Heimann, R.B. *Plasma Spray Coating Principles and Applications*; Wiley-VCH: Weinheim, Germany, 2008.
5. Fauchais, M.B.P.L.; Heberlein, J.V.R. Thermal Spray Fundamentals. In *From Powder to Part*; Springer: Greer, SC, USA, 2014.
6. Babu, P.S.; Sen, D.; Jyothirmayi, A.; Krishna, L.R.; Rao, D.S. Influence of microstructure on the wear and corrosion behavior of detonation sprayed Cr₂O₃-Al₂O₃ and plasma sprayed Cr₂O₃ coatings. *Ceram. Int.* **2018**, *44*, 2351–2357. [\[CrossRef\]](#)
7. Rao, K.S.; Girisha, K.; Shree, R.P.; Kumar, M. Effect of Surface Coatings on Thermal performance of steel Substrates. *Mater. Today Proc.* **2017**, *4*, 10249–10253. [\[CrossRef\]](#)
8. Kiilakoski, J.; Trache, R.; Björklund, S.; Joshi, S.; Vuoristo, P. Process Parameter Impact on Suspension-HVOF-Sprayed Cr₂O₃ Coatings. *J. Therm. Spray Technol.* **2019**, *28*, 1933–1944. [\[CrossRef\]](#)
9. Grimm, M.; Conze, S.; Berger, L.-M.; Drehmann, R.; Lampke, T. Microstructure and Properties of Atmospheric Plasma Sprayed (Al,Cr)₂O₃-TiO₂ Coatings from Blends. *J. Therm. Spray Technol.* **2021**, *31*, 256–268. [\[CrossRef\]](#)
10. Grimm, M.; Conze, S.; Berger, L.-M.; Paczkowski, G.; Lindner, T.; Lampke, T. Microstructure and Sliding Wear Resistance of Plasma Sprayed Al₂O₃-Cr₂O₃-TiO₂ Ternary Coatings from Blends of Single Oxides. *Coatings* **2020**, *10*, 42. [\[CrossRef\]](#)
11. Yang, X.; Zeng, J.; Zhang, H.; Wang, J.; Sun, J.; Dong, S.; Jiang, J.; Deng, L.; Zhou, X.; Cao, X. Correlation between microstructure, chemical components and tribological properties of plasma-sprayed Cr₂O₃-based coatings. *Ceram. Int.* **2018**, *44*, 10154–10168. [\[CrossRef\]](#)
12. Gerald, O.J.; Wenge, L.; Tao, Z.Y.; Long, L.C.; Qiang, L. Influence of plasma spraying current on the microstructural characteristics and tribological behaviour of plasma sprayed Cr₂O₃ coating. *Boletín Soc. Española Cerámica Vidr.* **2021**, *60*, 338–346. [\[CrossRef\]](#)
13. Toma, F.-L.; Potthoff, A.; Barbosa, M. Microstructural Characteristics and Performances of Cr₂O₃ and Cr₂O₃-15%TiO₂ S-HVOF Coatings Obtained from Water-Based Suspensions. *J. Therm. Spray Technol.* **2018**, *27*, 344–357. [\[CrossRef\]](#)
14. Li, N.-N.; Li, G.-L.; Wang, H.-D.; Kang, J.-J.; Dong, T.-S. Influence of TiO₂ content on the mechanical and tribological properties of Cr₂O₃-based coating. *Mater. Des.* **2015**, *88*, 906–914. [\[CrossRef\]](#)
15. Bastakys, L.; Marcinauskas, L.; Milieška, M.; Grigaliūnas, M.; Matkovič, S.; Aikas, M. Tribological Properties of Chromia and Chromia Composite Coatings Deposited by Plasma Spraying. *Coatings* **2022**, *12*, 1035. [\[CrossRef\]](#)
16. Mao, L.; Xiao, J.; Sun, G.; Wei, X.; Wu, D.; Cao, P.; Zhang, C. Microstructure and wear behaviors of Cr₂O₃-Al₂O₃ composite coatings deposited by atmospheric plasma spraying. *Surf. Coat. Technol.* **2022**, *444*, 128619. [\[CrossRef\]](#)
17. Bolelli, G.; Steduto, D.; Kiilakoski, J.; Varis, T.; Lusvarghi, L.; Vuoristo, P. Tribological properties of plasma sprayed Cr₂O₃, Cr₂O₃-TiO₂, Cr₂O₃-Al₂O₃ and Cr₂O₃-ZrO₂ coatings. *Wear* **2021**, *480*, 203931. [\[CrossRef\]](#)
18. Amanov, A.; Berkebile, S.P. Improvement in tribological behavior of thermal spray Cr₂O₃ and Cr₃C₂-NiCr coatings by ultrasonic nanocrystal surface modification. *Mater. Lett.* **2022**, *314*, 131919. [\[CrossRef\]](#)
19. Singh, V.P.; Sil, A.; Jayaganthan, R. Tribological behavior of plasma sprayed Cr₂O₃-3%TiO₂ coatings. *Wear* **2011**, *272*, 149–158. [\[CrossRef\]](#)

20. Ding, Q.; Zhao, G. Effects of CeO₂ on the microstructure and tribological properties of atmospheric plasma-sprayed Cr₂O₃-TiO₂ coatings. *Ind. Lubr. Tribol.* **2019**, *72*, 341–347. [[CrossRef](#)]
21. Hashemi, S.M.; Parvin, N.; Valefi, Z.; Alishahi, M. Comparative study on tribological and corrosion protection properties of plasma sprayed Cr₂O₃-YSZ-SiC ceramic coatings. *Ceram. Int.* **2019**, *45*, 21108–21119. [[CrossRef](#)]
22. Venturi, F.; Pulsford, J.; Hussain, T. A novel approach to incorporate graphene nanoplatelets to Cr₂O₃ for low-wear coatings. *Mater. Lett.* **2020**, *276*, 128283. [[CrossRef](#)]
23. Mukherjee, B.; Asiq Rahman, O.S.; Islam, A.; Sribalaji, M.; Keshri, A.K. Plasma sprayed carbon nanotube and graphene nanoplatelets reinforced alumina hybrid composite coating with outstanding toughness. *J. Alloys Compd.* **2017**, *727*, 658–670. [[CrossRef](#)]
24. Goyal, K.; Singh, H.; Bhatia, R. Behaviour of carbon nanotubes-Cr₂O₃ thermal barrier coatings in actual boiler. *Surface Eng.* **2019**, *36*, 124–134. [[CrossRef](#)]
25. Amudha, A.; Nagaraja, H.S.; Shashikala, H.D. Plasma-sprayed graphene oxide reinforced alumina composite coatings on low carbon steel with improved fracture toughness, brittleness index, and microhardness. *Mater. Today Proc.* **2021**, *39*, 1503–1508. [[CrossRef](#)]
26. Marcinauskas, L.; Mathew, J.S.; Milieška, M.; Aikas, M.; Kalin, M. Effect of graphite concentration on the tribological performance of alumina coatings. *J. Alloys Compd.* **2020**, *827*, 154135. [[CrossRef](#)]
27. Bagde, P.; Mehar, S.; Sapate, S.; Rathod, A. Effect of graphite addition on tribological behaviour of plasma sprayed Cr₂O₃-TiO₂ coating. *Mater. Today Proc.* **2022**, *56*, 2365–2370. [[CrossRef](#)]
28. Brinkienė, K.; Keželis, R.; Mečius, V. Effect of outlet nozzle design on the YSZ particle in-flight characteristics in plasma jet generated by DC plasma torch. In *Advances in Heat Transfer Engineering*; Begell House: Danbury, CT, USA, 2003; pp. 629–636.
29. Priyadershini, S.; Rahman, O.S.A.; Pandey, K.K.; Keshri, A.K. Remarkable improvement in tribological behavior of plasma sprayed carbon nanotube and graphene nanoplatelets hybrid reinforced alumina nanocomposite coating. *Ceram. Int.* **2019**, *45*, 5768–5778. [[CrossRef](#)]
30. Wang, L.; Liu, S.; Gou, J.; Zhang, Q.; Zhou, F.; Wang, Y.; Chu, R. Study on the wear resistance of graphene modified nanostructured Al₂O₃/TiO₂ coatings. *Appl. Surf. Sci.* **2019**, *492*, 272–279. [[CrossRef](#)]
31. Zamani, P.; Valefi, Z. Microstructure, phase composition and mechanical properties of plasma sprayed Al₂O₃, Cr₂O₃ and Cr₂O₃-Al₂O₃ composite coatings. *Surf. Coat. Technol.* **2017**, *316*, 138–145. [[CrossRef](#)]
32. Aruna, S.T.; Balaji, N.; Shedthi, J.; Grips, V.W.K. Effect of critical plasma spray parameters on the microstructure, microhardness and wear and corrosion resistance of plasma sprayed alumina coatings. *Surf. Coat. Technol.* **2012**, *208*, 92–100. [[CrossRef](#)]
33. Feng, Y.; Fang, J.; Wu, J.; Gu, K.; Liu, P. Mechanical and tribological properties of plasma sprayed graphene nanosheets/Al₂O₃+13 wt%TiO₂ composite coating. *Tribol. Int.* **2020**, *146*, 106233. [[CrossRef](#)]
34. Li, Y.; Liu, J.; Deng, J.; He, J.; Qin, Y.; Xing, Y.; Yin, F. Fabrication of graphene oxide reinforced plasma sprayed Al₂O₃ coatings. *Ceram. Int.* **2023**, *49*, 1667–1677. [[CrossRef](#)]
35. Liang, G.; Schmauder, S.; Lyu, M.; Schneider, Y.; Zhang, C.; Han, Y. An Investigation of the Influence of Initial Roughness on the Friction and Wear Behavior of Ground Surfaces. *Materials* **2018**, *11*, 237. [[CrossRef](#)] [[PubMed](#)]
36. Riedl, A.; Schalk, N.; Czettel, C.; Sartory, B.; Mitterer, C. Tribological properties of Al₂O₃ hard coatings modified by mechanical blasting and polishing post-treatment. *Wear* **2012**, *289*, 9–16. [[CrossRef](#)]
37. Conze, S.; Grimm, M.; Berger, L.-M.; Thiele, S.; Drehmann, R.; Lampke, T. Influence of simultaneous Cr₂O₃ and TiO₂ additions on the microstructure and properties of APS alumina coatings. *Surf. Coat. Technol.* **2021**, *405*, 126702. [[CrossRef](#)]
38. Harju, M.; Järn, M.; Dahlsten, P.; Nikkanen, J.-P.; Rosenholm, J.B.; Mäntylä, T. Influence of long-term aqueous exposure on surface properties of plasma-sprayed oxides Cr₂O₃ and Cr₂O₃-25 wt% TiO₂. *J. Colloid Interface Sci.* **2008**, *326*, 403–410. [[CrossRef](#)]
39. Zhao, X.; Li, S.; Hou, G.; An, Y.; Zhou, H.; Chen, J. Influence of doping graphite on microstructure and tribological properties of plasma sprayed 3Al₂O₃-2SiO₂ coating. *Tribol. Int.* **2016**, *101*, 168–177. [[CrossRef](#)]
40. Mahade, S.; Mulone, A.; Björklund, S.; Klement, U.; Joshi, S. Incorporation of graphene nano platelets in suspension plasma sprayed alumina coatings for improved tribological properties. *App. Surf. Sci.* **2021**, *570*, 151227. [[CrossRef](#)]

Disclaimer/Publisher's Note: The statements, opinions and data contained in all publications are solely those of the individual author(s) and contributor(s) and not of MDPI and/or the editor(s). MDPI and/or the editor(s) disclaim responsibility for any injury to people or property resulting from any ideas, methods, instructions or products referred to in the content.